Journal of Materials Chemistry B

Time-lapse imaging of cell death in cell culture and whole living organisms using turn-on deep-red fluorescent probes

Journal:	*Journal of Materials Chemistry B*
Manuscript ID	TB-ART-06-2018-001495.R1
Article Type:	Paper
Date Submitted by the Author:	07-Jul-2018
Complete List of Authors:	Jarvis, Tia; University of Notre Dame Roland, Felicia; University of Notre Dame Dubiak, Kyle; University of Notre Dame Huber, Paul; University of Notre Dame Smith, BD; University of Notre Dame,

Journal of Materials Chemistry B

ARTICLE

Time-lapse imaging of cell death in cell culture and whole living organisms using turn-on deep-red fluorescent probes†

Tia S. Jarvis,[a‡] Felicia M. Roland,[a‡] Kyle M. Dubiak,[a] Paul W. Huber,[a] and Bradley D. Smith[a]*

Received 00th January 20xx,
Accepted 00th January 20xx

DOI: 10.1039/x0xx00000x

www.rsc.org/

Cell death is a central process in developmental biology and also an important indicator of disease status and treatment efficacy. Two related fluorescent probes are described that are molecular conjugates of one or two zinc dipicolylamine (ZnDPA) coordination complexes with an appended solvatochromic benzothiazolium squaraine dye. The probes were designed to target the anionic phospholipid, phosphatidylserine (PS), that is exposed on the surface of dead and dying cells. A series of spectrometric and microscopy studies using liposomes and red blood cell ghosts as models showed that the probe with two ZnDPA targeting units produced higher affinity, stronger fluorescence "turn-on" effect, and better image contrast than the probe with one ZnDPA. Both fluorescent probes enabled "no-wash" time-lapse microscopic imaging of mammalian cell death within a culture. The probe with two ZnDPA units was used for non-invasive time-lapse imaging of cell death during the development of Xenopus laevis (frog) embryos. In vivo fluorescence micrographs revealed probe accumulation within the embryo tail, head and spine regions that were undergoing regression and apoptosis during growth and maturation. These new fluorescent probes are likely to be useful for time-resolved, non-invasive in vivo imaging of cell death process in range of living organisms. From a broader perspective, it should be possible to utilize the negative solvatochromism exhibited by benzothiazolium squaraine dyes for development of various "turn-on" deep-red fluorescent probes and materials that target cell surface biomarkers for in vitro and in vivo imaging.

Introduction

Cell death is a central step in a wide range of biological processes such as organism development, homeostasis, and self-defense.[1] In addition, cell death is a hallmark of many diseases including heart attack, neurodegeneration, autoimmune disease, and organ transplant failure.[2–4] There are several different forms of cell death, but the two most common are necrosis and apoptosis. Necrosis is a catastrophic event that is often caused by a mechanical or biochemical insult that disrupts the cell plasma membrane, releasing the intracellular contents and creating a local inflammatory response.[5] Conversely, apoptosis is often referred to as "programmed cell death" because it occurs in an organized and enzyme-dependent fashion.[6] Although these cell death process occur by quite different mechanisms, a common biomarker for both is exposure of the anionic phospholipid phosphatidylserine (PS) on the cell surface.[7] In the case of apoptosis, the exposed PS is recognized by phagocytes within the reticuloendothelial system that removes dead and dying cells without an influx of inflammatory cells. This immunological quiescence is a major reason why apoptosis is a central process in embryonic development events, such as morphogenesis.[8]

The last two decades has seen a substantial effort to develop molecular imaging agents that can be used to locate and monitor cell death processes in cell culture and in living subjects. Various cell death biomarker targeting strategies have been investigated including molecular probes that have selective affinity for surface exposed PS.[9] These molecular probes range from relatively large proteins and antibodies to peptides and synthetic molecules.[10] We have contributed to this effort by developing synthetic molecular probes that exploit the affinity of zinc dipicolylamine (ZnDPA) coordination complexes for the anionic head group of PS.[11] We have shown that fluorescent ZnDPA probes can selectively target the anionic PS-rich membrane surfaces that are a common structural feature of dead and dying mammalian cells, over neutral membrane surfaces which are characteristic of healthy cells. A range of fluorescent ZnDPA probes are known to selectively stain anionic dead/dying cells in cell culture and in small animal models of disease.[12 13 14] In most of these cases, the fluorescent reporter group acts as a signalling beacon, and image contrast is obtained after the unbound probe is removed by either washing the cell culture or waiting for clearance from the blood-pool of the living animal. There are many cell death imaging circumstances where this probe clearance step is inconvenient or impossible, and thus there is a need for new probes that are silent in bulk solution but "turn on" their signal at the site of cell death.[15] Furthermore, cell death probes with "turn-on" fluorescence can be incorporated into time-lapse (time-

[a] Department of Chemistry and Biochemistry, 236 Nieuwland Science Hall, University of Notre Dame, Notre Dame, IN 46556, USA.
* Email: smith.115@nd.edu
‡ T. S. J. and F. M. R. contributed equally to this work.
†Electronic Supplementary Information (ESI) available: Probe synthesis and spectral characterization, cell microscopy images, cell viability, and Xenopus embryo images. See DOI: 10.1039/x0xx00000x

resolved) imaging protocols that aim to characterize the dynamics of cell death procesess in cell culture and whole living organisms.[16]

To date, several different fluorescence activation strategies have been explored that target intracellular or extracellular cell death biomarkers.[17] [18] In the specific case of "turn-on" fluorescent probes that target exposed PS, there are published cell studies using visible wavelength dyes,[19] or probes that exploit concentration dependent aggregation effects,[20] [21] but no demonstration of utility for in vivo imaging (*i.e.*, imaging of the dead/dying cells in a living subject).

The aim of this study was to develop deep-red fluorescent ZnDPA probes that bind to the surface of dead and dying cells and exhibit "turn-on" fluorescence. The practical goal was to demonstrate "no-wash" imaging of cell death in a cell culture and also time-lapse in vivo imaging of cell death in a living organism. To achieve the desired fluorescence turn-on effect, we chose to append a solvatochromic fluorescent dye to a ZnDPA targeting unit. While many solvatochromic fluorescent dyes are known, there are very few that operate in the deep-red wavelengths that are most suitable for in vivo imaging.[22] For several years we have been working with symmetrical squaraine dyes that have two identical π-electron donor groups (D) connected to a central acceptor (A) to yield a D-A-D structure. These dyes exhibit high favorable qualities for fluorescence imaging including narrow and intense deep-red or near-infrared absorption bands, and high fluorescence quantum yields.[23] In this current study, we employ an unsymmetrical benzothiazolium squaraine dye, which has two different donor groups (D_1-A-D_2, $D_1 \neq D_2$) and exhibits unusual negative solvatochromism; that is, increasing absorbance wavelength in decreased solvent polarity.[24] [25] Furthermore, the fluorescence quantum yield is increased when a benzothiazolium squaraine dye is transferred from water to a less polar organic solvent.[26] [27] Since probe binding to a membrane surface is equivalent to probe transfer from water to a less polar microenvironment,[28] we felt that the combination of these two spectral effects could be combined synergistically to create new and unique PS-targeting probes that identify the surfaces of dead and dying cells with "turn-on" fluorescence. In the following sections we describe the design and synthesis of two related fluorescent probes, and a sequential series of probe performance studies that evaluated: (a) PS targeting properties using model liposomes and red blood cell ghosts, (b) "no-wash" fluorescence microscopic imaging of dead and dying cells within a culture, and (c) time-lapse in vivo fluorescence imaging of cell death during the development and maturation of *Xenopus laevis* (frog) embryos.

Results and discussion

Probe design and characterization

In **Figure 1** is the chemical structure of the precursor unsymmetrical benzothiazolium squaraine (**USQ**) dye which has an appended triethylene glycol chain to enhance water solubility and attenuate dye self-aggregation. Also shown are chemical structures of the two fluorescent probes, ZnDPA unsymmetrical squaraine (**ZnDPA-USQ**) with one coordinated zinc(II) cation, and bisZnDPA unsymmetrical squaraine (**BZnDPA-USQ**) with two coordinated zinc(II) cations. The coordinated zinc cations mediate reversible association with various polyanionic phosphorylated molecules and also bilayer membranes containing anionic PS.[11] The affinity of ZnDPA probes for PS-rich membranes is sensitive to microenvironment effects, such as acidic pH, and attenuated by the presence of competing polyphosphates. But in standard physiological conditions there is always high probe selectivity for the anionic surface of dead/dying cells over the neutral surface of healthy cells.[11-14] As a general trend bisZnDPA probes with two coordinated zinc cations, like **BZnDPA-USQ**, exhibit higher affinity and selectivity for dead/dying cell surfaces than a ZnDPA probe with one zinc cation like **ZnDPA-USQ**.[14] The compound synthesis is described in the Electronic Supplementary Information along with spectral proof of structure and high purity.

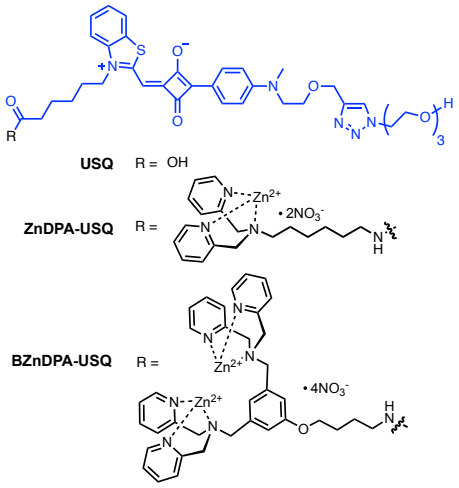

Fig. 1. Structures of untargeted control dye (**USQ**), and targeted molecular probes **ZnDPA-USQ** and **BZnDPA-USQ**.

In **Table 1** is a listing of absorption and emission maxima for the three compounds in four solvents of different polarities. As expected, the unmodified **USQ** exhibited negative solvatochromism with a red shift in λ_{max} as the solvent polarity was decreased from H_2O to DMSO.[27] Additionally, the fluorescence quantum yield in water (φ_f = 0.11) was lower than the less polar butanol (φ_f = 0.32).[28] The same spectral trend was observed with **ZnDPA-USQ** and **BZnDPA-USQ (Figure S1)**, but in water the optical properties for the two probes were affected by probe self-aggregation. We have reported previously that self-aggregation of fluorescent ZnDPA probes produces broadened and red-shifted absorption bands and lower fluorescence quantum yields.[14] Proof that the two probes exist in water as a mixture of self-aggregated and deaggregated species was gained by conducting simple titration experiments that added pyrophosphate (PPi) to the probe samples.[29] [30] The highly anionic PPi has a high affinity for ZnDPA units and forms a complex that favors a deaggregated state (most likely a monomeric probe molecule as illustrated in Figure 2A). The

titration profiles in **Figure 2B-D** show that incremental addition of PPi had no effect on **USQ** absorption but eliminated the red-shifted self-aggregation bands for the two ZnDPA probes, with a larger effect seen with **BZnDPA-USQ** indicating a higher degree of probe self-aggregation.

The expected high photostability of the benzothiazolium squaraine fluorophore was confirmed by conducting experiments that illuminated separate cuvette samples of each probe with red-light from a Xenon lamp. In each case, there was negligible change in probe absorbance (**Figure S2**) indicating very high photostability which is a crucial feature for time-lapse imaging experiments.

Table 1. Spectral properties of fluorescent probes (2 μM) in water, methanol, butanol, and DMSO.[a]

Solvent	Water		Methanol		Butanol		DMSO	
ET(30) [kcal/mol][31 32]	63.1		55.5		47.1		45.1	
	Abs (nm)	Em (nm)	Abs (nm)	Em (nm)	Abs (nm)	Em (nm)	Abs (nm)	Em (nm)
USQ	551	656	592	656	601	656	608	676
ZnDPA-USQ	547	663	593	662	599	659	608	677
BZnDPA-USQ	583	663	595	663	606	665	608	676

[a]Fluorescence quantum yield for **USQ** = 0.11 in water and 0.32 in butanol. The fluorescence quantum yields for **ZnDPA-USQ** and **BZnDPA-USQ** are strongly affected by probe self-aggregation which depends on concentration, solvent polarity, and identity of probe counter anions.

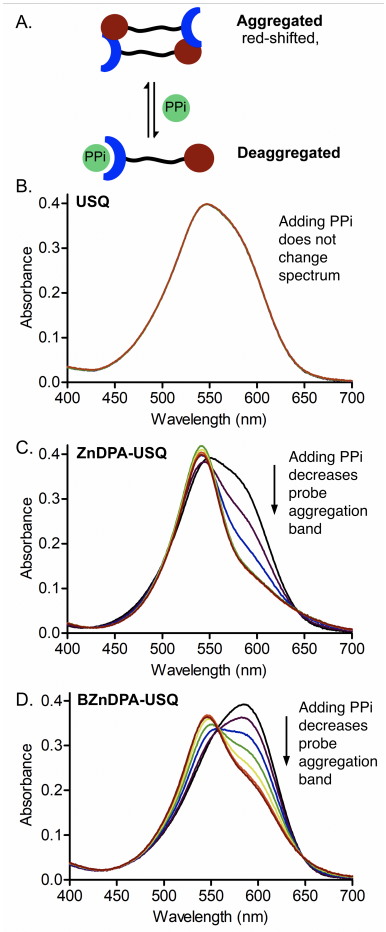

Fig. 2. (A) Schematic picture of probe deaggregation caused by association of probe ZnDPA units with PPi. Changes in absorption profiles for: (B) **USQ**, (C) **ZnDPA-USQ**, and (D) **BZnDPA-USQ** (10 μM) in water caused by titration of pyrophosphate (PPi) at 0.5 μM increments

Liposome binding studies

The capabilities of **ZnDPA-USQ** and **BZnDPA-USQ** to target PS-rich membranes and "turn-on" fluorescence was demonstrated by conducting a series of liposome titration studies. Two liposome compositions were utilized; zwitterionic liposomes comprised entirely of 1-palmitoyl-2-oleoyl-sn-glycero-3-phosphocholine (POPC) were designed to mimic the uncharged membrane surfaces of healthy cells, and anionic liposomes comprised of POPC and (1-palmitoyl-2-oleoyl-sn-glycero-3-phosphoserine (POPS) in an 80:20 ratio were designed to mimic the PS-rich membrane surfaces of dead and dying cells. Shown in **Figure 3A,B** are the absorbance and emission spectra of **ZnDPA-USQ** and **BZnDPA-USQ** in water, and in the presence of zwitterionic or anionic liposomes. As expected, the absorbance profile of each probes in the presence of zwitterionic liposomes was similar to that in water indicating no significant binding to the liposome surface.[14] In the presence of anionic liposomes, the **ZnDPA-USQ** probe exhibited a strong red-shift in absorbance maxima and moderate "turn-on" fluorescence, indicating deaggregated probe binding to the liposomes and transfer of the appended squaraine dye from bulk water to a less polar microenvironment on the membrane surface.[28] The spectra for **BZnDPA-USQ** probe in the presence of anionic liposomes differed in that there was only a small red-shift in absorbance maxima and very strong "turn-on" fluorescence. The equilibrium picture that explains all these liposome results is shown in **Figure 4**. In bulk water the **ZnDPA-USQ** probe exists as a mixture of self-aggregated and deaggregated species and association of deaggregated species (free probe) with the surface of anionic liposomes produces a red-shift in absorption along with enhanced fluorescence quantum yield (caused by the negative solvatochromic effect). The **BZnDPA-USQ** probe, with two ZnDPA units, is more extensively self-aggregated in bulk water which produces a red-shifted absorbance, self-quenching, and low fluorescence.[14] Association of **BZnDPA-USQ** with the anionic liposomes is quite favored because it has two ZnDPA units. Although the two-step binding process that converts self-aggregated **BZnDPA-USQ** in water to membrane-bound probe produces little change in absorption wavelength there is a large enhancement of probe fluorescence quantum yield (caused by probe deaggregation effect).

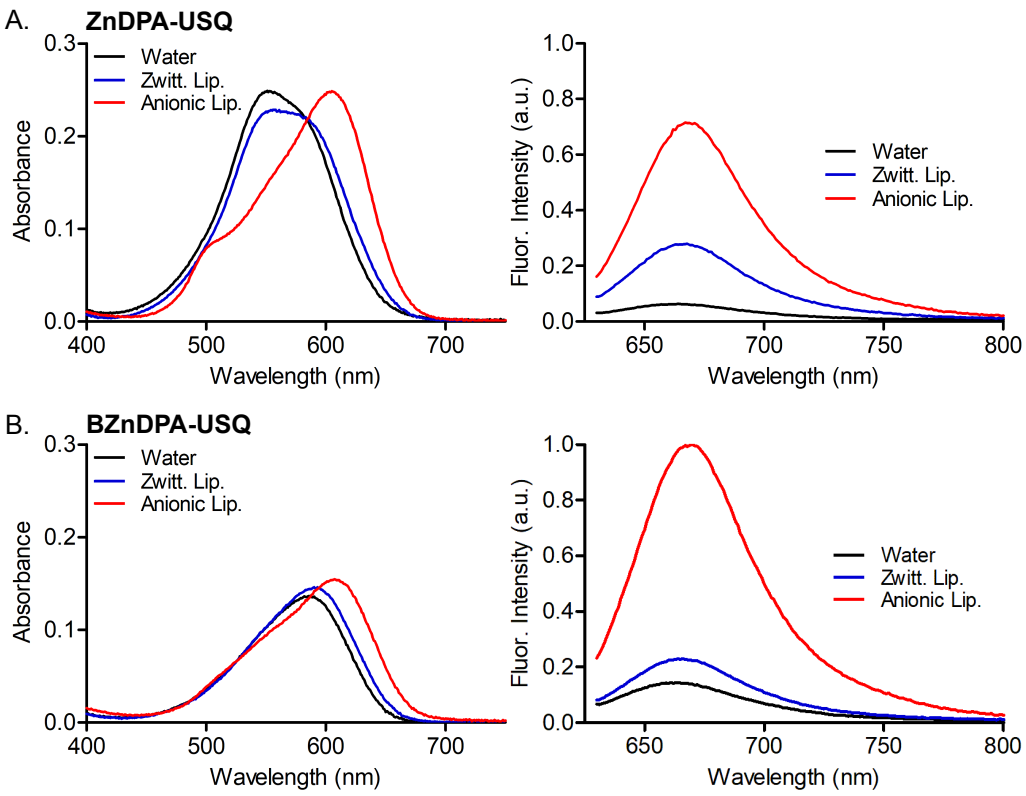

Fig. 3. Absorption and emission (ex: 619 nm) spectra for: (A) **ZnDPA-USQ** or (B) **BZnDPA-USQ** (10 µM), in water, or in the presence of zwitterionic liposomes (100% POPC, 1 mM) or anionic liposomes (80% POPC, 20% POPS, 1 mM).

No-wash microscopic imaging of red blood cell ghosts

It is relatively straightforward to convert red blood cell (RBCs) into inside-out "RBC ghosts" that do not contain hemoglobin and have PS exposed on the exterior membrane surface.[33] RBC ghosts have an average diameter of ~10 µm and are excellent mimics of aging RBCs and apoptotic cells.[34 35] To evaluate probe capability for "turn-on" fluorescence and no wash imaging, separate samples of inside-out RBC ghosts were prepared and treated with **ZnDPA-USQ** or **BZnDPA-USQ**. Shown in **Figure 5A** are fluorescence micrographs of the samples acquired at 2, 3, 4, 5, and 15 minutes after probe addition (500 nM). In **Figure S3** is another set of time-lapse micrographs acquired at higher probe concentration (10 µM). Both sets of micrographs clearly show an improvement in image contrast over time due to increasing probe accumulation on the surface of the RBC ghosts with accompanying "turn-on" fluorescence. In **Figure 5B** is a quantitative comparison of the signal-to-background ratio (S/B) at 2 and 15 minutes. The RBC ghosts treated with **BZnDPA-USQ** exhibited a larger increase in S/B reflecting the probe's higher affinity for PS-rich membranes and its capacity for higher "turn-on" fluorescence.

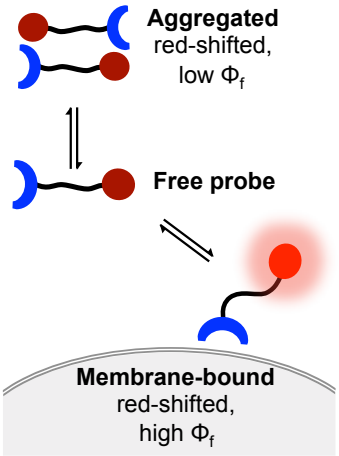

Fig. 4. Generalized scheme showing the equilibria for association of **ZnDPA-USQ** or **BZnDPA-USQ** with anionic PS-rich membranes.

No-wash microscopic imaging of mammalian cell death

The goal of the first set of in vitro mammalian cell experiments was to determine if the fluorescent probes could distinguish dead/dying cells from healthy cells. Microscopy experiments examined an experimentally convenient culture of CHO-K1 cells treated with Staurosporine, a non-selective inhibitor of protein kinases that induces cell apoptosis. After incubation with the Staurosporine for 3 hours, separate samples of the cells were treated with two different concentrations of **ZnDPA-USQ** or **BZnDPA-USQ** (500 nM or 10 µM), followed by a washing step and treatment with a blue-emitting nuclear stain (Hoechst33342) and a green-emitting live

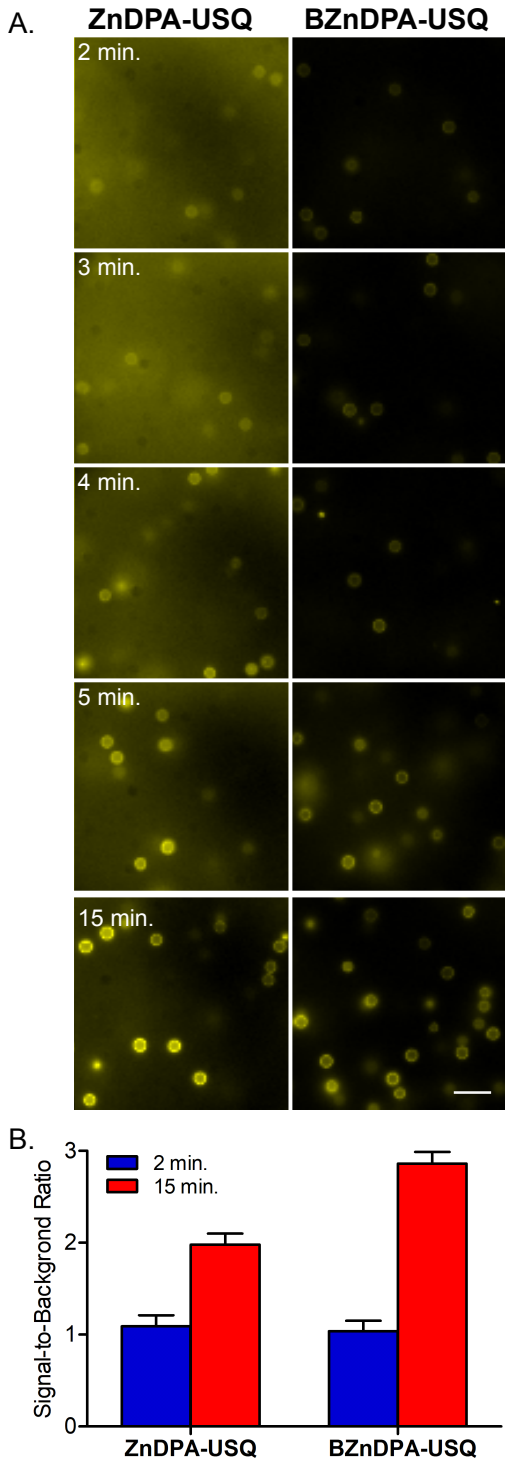

Fig. 5. Time-lapse imaging of fluorescent probe binding to the surface of RBC ghosts. (A) Fluorescence micrographs of RBC ghosts treated with 500 nM **ZnDPA-USQ** or **BZnDPA-USQ** and imaged at subsequent time intervals using a standard TxRed filter set. (B) Quantification of the signal-to-background ratio for the micrographs at 2 and 15 minutes after probe treatment. Scale bar = 25 µm.

cell indicator (CalceinAM). Control experiments used CHO-K1 cells that did not receive Staurosporine treatment. Inspection of the representative micrographs in **Figure 6** shows that at 10 µM both the **ZnDPA-USQ** and the **BZnDPA-USQ** probes selectively stained the apoptotic cells and not the healthy cells labeled with CalceinAM. Replicate experiments at lower probe concentration (500 nM) found that **BZnDPA-USQ** stained dead/dying cells more intensely than **ZnDPA-USQ** (**Figure S4**), a difference that is attributed to the higher affinity of **BZnDPA-USQ** for exposed PS in the dead/dying cell membranes.

The next set of mammalian cell experiments assessed probe capability for no wash microscopic imaging of cell death. The goal was to demonstrate time-lapse imaging of cell death. The cell death process was achieved by simply removing CHO-K1 cells from the humidified incubator environment (37 °C, 5% CO_2), placing them under phosphate buffered saline, and monitoring them while exposed to normal lab atmosphere and temperature (21.5 °C). It is not surprising that the cumulative stress of these conditions slowly induces cell death.[36 37 38] Shown in **Figure 7A** are representative micrographs of two populations of cells that were tracked over 80 minutes. One population was treated with **ZnDPA-USQ** and the other with **BZnDPA-USQ**. In both cases, probe fluorescence "turned-on" over time at the surface of cells as they began to die. The yellow arrows in the micrographs highlight individual cells undergoing apoptosis and forming apoptotic bodies.[39] Conversely, the blue arrows point to cells undergoing necrosis which is characterized by cytoplasmic swelling.[40] In **Figure 7B** is the quantification of fluorescence signal-to-background ratio for each probe as a function of time. The plots indicate that the higher affinity **BZnDPA-USQ** probe binds to dying cells earlier in the time course than the **ZnDPA-USQ** probe.

The excellent imaging performance of **BZnDPA-USQ** suggested that it was highly suitable for in vivo imaging studies. Before conducting in vivo experiment, we evaluated probe toxicity in CHO-K1 cells using a standard MTT toxicity assay. Initial testing incubated the cells with different probe concentrations for 24 hours. As shown in **Figure S5**, there was no detectable toxicity with **BZnDPA-USQ** concentrations up to 40 µM.

Time-lapse fluorescence imaging of apoptosis during xenopus embryo morphogenesis

The development of an *Xenopus laevis* embryo into a tadpole is commonly studied by developmental biologists as an experimental model of early morphogenesis.[41] We hypothesized that **BZnDPA-USQ** could be used for non-invasive time-lapse imaging of cell death during embryonic development. We incubated *Xenopus* embryos (stage 26) in a solution of 30 µM **BZnDPA-USQ** in Marc's Modified Ringer's buffer (1/3 MMR) at 22 °C. After 24 hours (stage 36/37), the embryos were removed and imaged using a fluorescence microscope to determine the location of the **BZnDPA-USQ** probe. The images in **Figure 8** reveal high probe fluorescence around the tail, head, and spine regions which are known to undergo partial regression and apoptosis during growth and maturation.[42]

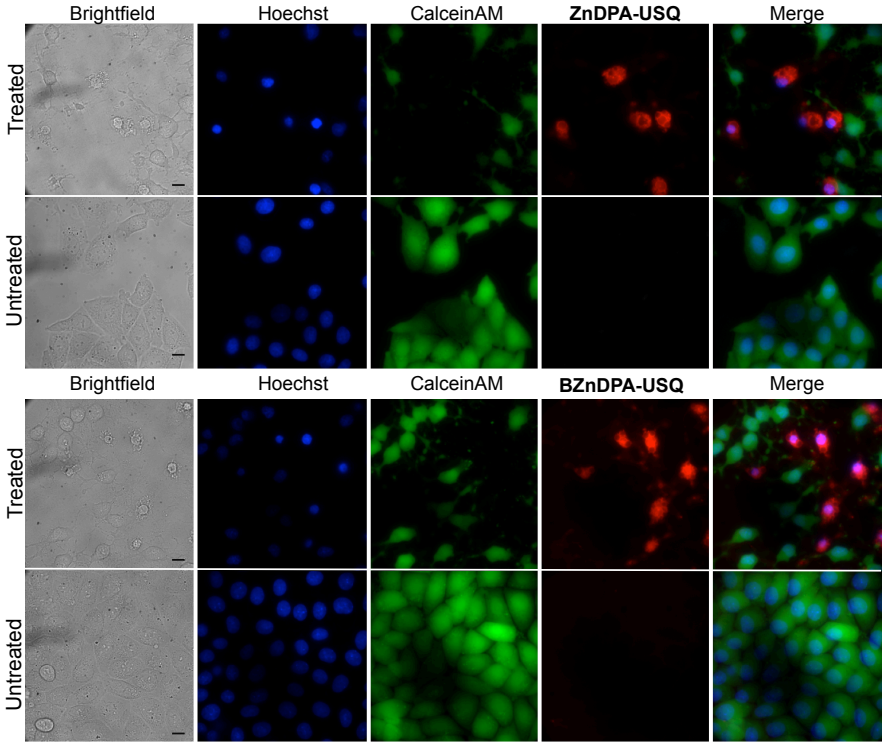

Fig. 6. Fluorescence micrographs of CHO-K1 cells that had been treated with Staurosporine (500 nM) for 3 hours or were untreated. The cells were subsequently treated with fluorescent probes **ZnDPA-USQ** or **BZnDPA-USQ** (red, 10 μM) that selectively stained the dead/dying cells, nuclear stain Hoechst33342 (blue, 3 μM), and live cell indicator CalceinAM (green, 5 μM) (Scale bar = 50 μm).

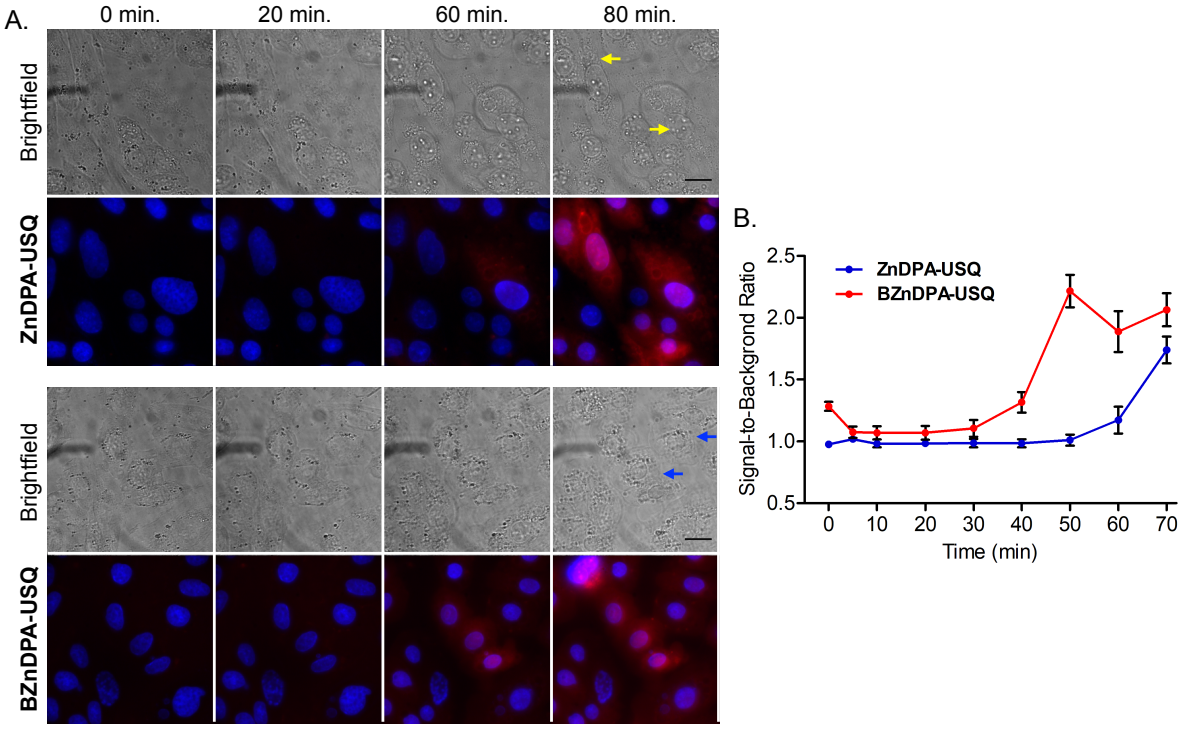

Fig. 7. (A) Brightfield and fluorescence micrographs of CHO-K1 cells undergoing slow cell death over 80 minutes, as indicated by "turn on" of deep-red fluorescence (detected using a standard TxRed filter set) for **ZnDPA-USQ** or **BZnDPA-USQ** (10 μM). Necrotic and apoptotic cells are indicated with blue and yellow arrows, respectively. Cell nuclei are stained with blue-emitting Hoechst33342. Scale bar = 50 μm. (B) Quantification of the change in signal-to-background ratio over time for the probe's deep-red fluorescence.

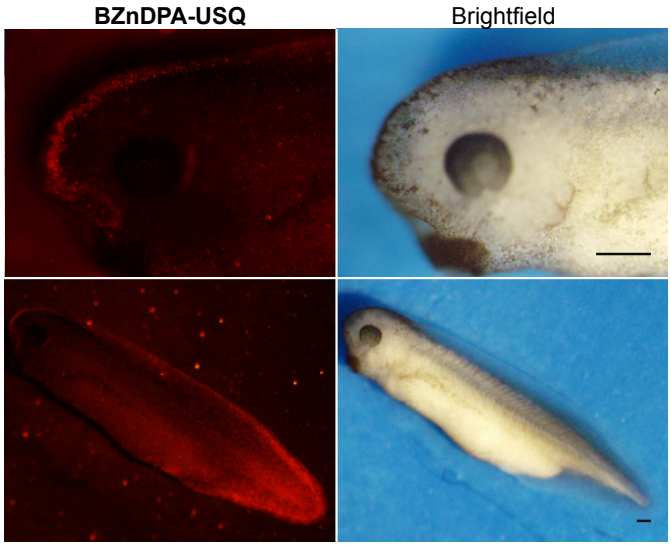

Fig. 8. Deep-red fluorescence (left) and brightfield (right) images of *Xenopus* embryo (stage 36/37) after 24 hours of incubation in **BZnDPA-USQ** (30 μM) showing location of apoptotic cells. Scale bar = 0.2 mm

We next performed an experiment that assessed the suitability of targeted **BZnDPA-USQ** for imaging embryo development over time. To do this, separate cohorts of embryos were placed in either a 1/3 MMR solution containing 30 μM of **BZnDPA-USQ** or control **USQ**. The embryos were kept in the medium at 22 °C for 16 hours (stage 32), then removed and imaged. After imaging, the embryos were placed in probe-free 1/3 MMR solution at 22 °C and imaged again after 8 hours (stage 36/37) and 30 hours (stage 41). In the case of untargeted **USQ** there was negligible deep-red fluorescence within the embryo at all time points. In contrast, there was significant accumulation of **BZnDPA-USQ** in the embryos after the 16 hour incubation, with deep-red fluorescence throughout the embryo. At the later time periods, the fluorescence had localized largely to the apoptotic tail region (**Figure S6**). As shown by the brightfield images in **Figure S7**, embryos bathed in **BZnDPA-USQ** or probe-free 1/3 MMR solution for periods up to 46 hours were healthy with no evidence of probe toxicity.

Experimental

Synthesis, structure, and characterization

Detailed synthetic procedures to make **USQ**, **ZnDPA-USQ**, and **BZnDPA-USQ** are described in the Electronic Supplementary Information along with spectral data proving structural identity and high product purity. Pyrophosphate titration experiments added aliquots from a stock solution of PPi (Sigma) in water to a 10 μM aqueous solution of **USQ**, **ZnDPA-USQ**, or **BZnDPA-USQ**.

Liposome binding studies

Liposome preparation. Appropriate ratios of 1-palmitoyl-2-oleoyl-sn-glycero-3-phosphocholine (POPC) and 1-palmitoyl-2-oleoyl-sn-glycero-3-phosphoserine (POPS) were mixed together in $CHCl_3$ and the solvent removed by N_2 stream for 5 minutes at room temperature, followed by a high vacuum for 2 hours. The remaining film was hydrated and vortexed for 1 minutes, then subjected to 10 freeze-thaw cycles using liquid N_2 and a 40 °C water bath. The liposomes were extruded 23 times through a membrane (polycarbonate, 200 nm pore size) at room temperature and used immediately after preparation.

Red blood cell ghost studies

RBC ghost preparation. Whole red blood was collected from Balb/c mice at the Friemann Life Science Center. Fresh blood was treated with anticoagulant heparin (1000 U/mL, 0.1 mL/syringe) and kept on ice until use. In a sterile 1.5 mL eppendorf tube, 50 μL of whole blood was added to and rinsed 3x with ice cold isotonic buffer (0.9% NaCl) by centrifugation to remove plasma proteins and buffy coat (5000 rpm, 5-10 min.). Cells were subsequently treated with ice cold hypotonic buffer (0.6% NaCl), vortexed 10 seconds, and kept on ice for 20 minutes. Hemoglobin was removed via centrifugation at 10,000 rpm for 15 minutes. Residual hemoglobin (cells remaining slightly red) was removed by repeating the hypotonic incubation/centrifugation step until the RBC ghosts appeared almost colorless. RBC ghosts were kept in isotonic buffer at 4 °C for up to one week.

RBC ghost microscopy. RBC ghosts were diluted into an 8-well chambered coverglass using sterile H_2O. Immediately before imaging, **ZnDPA-USQ** or **BZnDPA-USQ** was added to yield a final probe concentration of either 500 nM or 10 μM. The

ghosts were gently mixed using a pipette to evenly distribute the fluorescent probe and then allowed to settle for one minute. Microscopic images were obtained once every minute for 5 minutes and again at 15 minutes using a Zeiss Axiovert epifluorescence microscope equipped with a TxRed filter set (ex: 562/40, em: 624/40).

Mammalian cell culture studies

Cell culture. Chinese Hamster Ovary (CHO-K1) cells were cultured in F-12K media supplemented with 10% fetal bovine serum and 1% streptomycin/penicillin in a humidified incubator at 37 °C, 5% CO_2. Cells were seeded in an 8-well chambered coverglass and grown to 80% confluency.

Staurosporine treatment microscopy. Cells were treated with 500 nM staurosporine in complete media for 3 hours. The media was carefully removed and cells were rinsed with warm PBS before staining with a CalceinAM (5 μM) and Hoechst33342 (3 μM) for 10 minutes at 25 °C and protected from light. The cells were again carefully rinsed with warm PBS and covered with phenol red-free Opti-MEM Reduced Serum Medium (Gibco™). A 200 μL aliquot of **ZnDPA-USQ** or **BZnDPA-USQ** (to achieve a final concentration of 500 nM or 10 μM) was added to each individual well immediately prior to microscopic imaging.

Environmental induced cell death microscopy. Media was removed and cells were stained with Hoechst33342 (3 μM) in phosphate buffered saline (PBS) for 10 minutes at 25 °C, protected from light. The cells were rinsed twice with PBS and covered with PBS at 21.5 °C with exposure to the lab atmosphere. An aliquot of **ZnDPA-USQ** or **BZnDPA-USQ** was added to each microwell to give a final probe concentration of 10 μM immediately prior to imaging. The cells were then imaged every 10 minutes for 80 minutes to monitor cell death events.

Fluorescence microscopy and image analysis. Fluorescent micrographs were acquired using a Zeiss Axiovert epifluorescence microscope equipped with the following filter sets: UV (ex: 387/11, em: 447/60), FITC (ex: 485/20, em: 524/24), TxRed (ex: 562/40, em: 624/40), Cy5.5 (ex: 655/40, em: 716/40). ImageJ Software was used to process fluorescent images. To determine the signal-to-background ratio (S/B), the fluorescence intensity of all images in a set was first normalized. The mean pixel intensity (MPI) was found for ten different ROIs (2x2 pixels), where the region for signal (S) was a fluorescent cell and the region for background (B) was a non-fluorescent cell.

Cell toxicity measurements. The toxicity of **BZnDPA-USQ** was determined using a MTT cell viability assay. CHO-K1 cells were cultured in F-12K media supplemented with 10% fetal bovine serum and 1% streptomycin/penicillin in a humidified incubator at 37 °C, 5% CO_2. Cells were seeded in a 96-well plate and grown to 80% confluency. The manufactures protocol for the Vybrant MTT assay (Invitrogen Eugene, USA) was followed. Briefly, culture media was removed from cells and replaced with various concentrations of **BZnDPA-USQ**, ranging from 500 nM to 40 μM, and incubated for 24 hours (n=3) at 37 °C, 5% CO_2. After incubation, the probe solution was removed and replaced with 110 uL of culture medium containing [3-(4,5-dimethylthiazol-2-yl)-2,5-diphenyltetrazolium bromide] (MTT, 5 mg/mL) and incubated for 4 hours at 37 °C, 5% CO_2. Next, 100 μL of a SDS-HCl solution (10 mg/mL) was added to each well and incubated for 4 hours at 37 °C, 5% CO_2. The colorimetric change was quantified by reading the absorbance at 572 nm. Data was normalized to cells that were treated with fresh media instead of **BZnDPA-USQ**. To determine toxicity of **BZnDPA-USQ** at longer exposure times, cells were incubated for various periods with the dye (30 μM) from 24 to 72 hours. Incubation periods were timed such that all periods would be finished at once. Each condition was normalized to its corresponding control, which was incubated with fresh media instead of dye for that period.

Xenopus embryo imaging studies

Xenopus embryo preparation. All procedures were performed in accordance to the Notre Dame Institutional Animal Care and Use Committee (IACUC Protocol: 18-02-4408). Prior to spawning, a female *frog* was injected with 600 units of human chorionic gonadotropin. Once eggs were collected, 1/3 of whole teste was minched and added to the eggs in a 1/3 diluted solution of Marc's Modified Ringer's (1/3 MMR) buffer for 30 minutes. Embryos were dejellied using a 2% cysteine solution pH 8.0 for 4 mins, followed by multiple washes in 1/3 MMR buffer. Embryos were kept at 22 °C.

Xenopus embryo imaging. At 26 hours post fertilization (stage 24), an embryo was placed into a solution of BZnDPA-USQ or USQ (30 μM) in 1/3 MMR and the samples allowed to grow at 22 °C. For the first experiment, the embryos were removed from the medium after an additional 24 hours (stage 36/37) and imaged using an Olympus SZX16 Reflected Fluorescence System (SZX2-FRFP1 filter set, ex: 540/20, Em: 575/10). For the second experiment, the stage 24 embryos were placed in a solution of BZnDPA-USQ or USQ (30 μM) in 1/3 MMR, allowed to grow at 22 ^{o}C for 16 hours (stage 32), then removed and imaged using the same setup. After imaging, the embryos were placed back into fresh, probe-free 1/3 MMR solution and the incubation was continued. After additional incubation periods of 8 hours (stage 36/37) and 30 hours (stage 41) the embryos were removed and imaged. An anesthetic (0.33 mg/mL cisatracurium in 1/3 MMR buffer) was used to immobilize the embryos at the final time point.

Conclusions

Two targeted molecular probes were prepared and evaluated as “turn on” deep-red fluorescent probes for cell death imaging. Each probe structure was comprised of a solvatochromic benzothiazolium squaraine dye with one or two appended ZnDPA targeting units that have affinity for the anionic PS that is exposed on the exterior surface of dead and dying cells. A series of spectrometric and microscopy studies using model liposomes and RBC ghosts showed that the probe **BZnDPA-USQ** with two ZnDPA targeting units produced higher affinity, stronger fluorescence “turn-on” effect, and better image contrast than the probe **ZnDPA-USQ** with one ZnDPA. Both fluorescent probes enabled “no-wash” time-lapse

microscopic imaging of mammalian cell death within a culture. In addition, **BZnDPA-USQ** was used for non-invasive time-lapse imaging of cell death during the development and early morphogenesis of Xenopus laevis (frog) embryos. In vivo fluorescence micrographs revealed probe accumulation around the embryo head, tail and spine regions, which are known to undergo regression and apoptosis during metamorphosis. Taken together, the results suggest that **BZnDPA-USQ** is a promising new fluorescent probe for time-lapse imaging of cell death process in a range of organisms that are studied extensively as models of biological development, disease progression, and efficacy of disease treatment. From a broader perspective, it should be possible to exploit the negative solvatochromism exhibited by benzothiazolium squaraine dyes for the design and fabrication of various "turn-on" deep-red fluorescent probes and materials that target cell surface biomarkers.

Conflicts of interest

There are no conflicts to declare.

Acknowledgements

This work was supported by grants from the NSF (CHE1708240 to B.D.S.) and the NIH (R01GM059078 to B.D.S., T32GM075762 to F.M.R. and R01HD084399 to P.W.H.).

Notes and references

1 J. C. Ameisen, *Cell Death Differ.*, *2002*, **9**, 367.
2 R. A. Lockshin and Z. Zakeri, *J. Cell. Mol. Med.*, *2007*, **11**, 1214–1224.
3 D. Kabelitz, *Transplantation*, *1998*, **65**, 869.
4 A. M. Gorman, *J. Cell. Mol. Med.*, *2008*, **12**, 2263.
5 P. Davidovich, C. J. Kearney and S. J. Martin, *Biol. Chem.*, *2014*, **395**, 1163.
6 G. Kroemer, L. Galluzzi, P. Vandenabeele, J. Abrams, E. S. Alnemri, E. H. Baehrecke, M. V Blagosklonny, W. S. El-Deiry, P. Golstein, D. R. Green, M. Hengartner, R. A. Knight, S. Kumar, S. A. Lipton, W. Malorni, G. Nuñez, M. E. Peter, J. Tschopp, J. Yuan, M. Piacentini, B. Zhivotovsky, and G. Melino, *Cell Death Differ.*, *2009*, **16**, 3.
7 B. Sharma and S. S. Kanwar, *Semin. Cancer Biol.*, *2017*, DOI:10.1016/J.SEMCANCER.2017.08.012.
8 A. Glucksmann, *Biol. Rev.*, *1951*, **26**, 59.
9 A. A. Neves and K. M. Brindle, *J. Nucl. Med.*, *2014*, **55**, 1.
10 B. A. Smith and B. D. Smith, *Bioconjug. Chem.*, *2012*, **23**, 1989.
11 D. R. Rice, K. J. Clear and B. D. Smith, *Chem. Commun.*, *2016*, **52**, 8787.
12 B. A. Smith, K. M. Harmatys, S. Xiao, E. L. Cole, A. J. Plaunt, W. Wolter, M. A. Suckow and B. D. Smith, *Mol. Pharm.*, *2013*, **10**, 3296.
13 A. J. Plaunt, K. M. Harmatys, W. R. Wolter, M. A. Suckow and B. D. Smith, *Bioconjug. Chem.*, *2014*, **25**, 724.
14 K. J. Clear, K. M. Harmatys, D. R. Rice, W. R. Wolter, M. A. Suckow, Y. Wang, M. Rusckowski and B. D. Smith, *Bioconjug. Chem.*, *2016*, **27**, 363.
15 W. Zeng, X. Wang, P. Xu, G. Liu, H. S. Eden and X. Chen, *Theranostics*, *2015*, **5**, 559.
16 G. C. Forcina, M. C. Conlon, A. Wells, J. Y. Cao, S. J. Dixon, *Cell Systems* , *2017*, **4** , 600.
17 H. Shi, R. T. K. Kwok, J. Liu, B. Xing, B. Z. Tang and B. Liu, *J. Am. Chem. Soc.*, *2012*, **134**, 17972.
18 G. Saranya, P. Anees, M. M. Joseph, K. K. Maiti and A. Ajayaghosh, *Chem. Eur. J.*, *2017*, **23**, 7191.
19 B. I. Murcar-Evans, A. D. Cabral, K. Toutah, E. D. de Araujo, A. Lai, P. M. Macdonald, A. Berger-Becvar, D. Kraskouskaya and P. T. Gunning, *Analyst*, *2017*, **142**, 4511.
20 Q. Hu, M. Gao, G. Feng, X. Chen and B. Liu, *ACS Appl. Mater. Interfaces*, *2015*, **7**, 4875.
21 A. C. S. Leung, E. Zhao, R. T. K. Kwok, J. W. Y. Lam, C. W. T. Leung, H. Deng and B. Z. Tang, *J. Mater. Chem. B*, *2016*, **4**, 5510.
22 A. S. Klymchenko, *Acc. Chem. Res.*, *2017*, **50**, 366.
23 S. Sreejith, P. Carol, P. Chithra and A. Ajayaghosh, *J. Mater. Chem.*, *2008*, **18**, 264
24 F. Terenziani, A. Painelli, C. Katan, M. Charlot and M. Blanchard-Desce, *J. Am. Chem. Soc.*, *2006*, **128**, 15742.
25 C. Reichardt, *Chem. Rev.*, *1994*, **94**, 2319.
26 K. M. Shafeekh, M. S. Soumya, M. A. Rahim, A. Abraham and S. Das, *Photochem. Photobiol.*, *2014*, **90**, 585.
27 K. M. Shafeekh, S. Das, C. Sissa and A. Painelli, *J. Phys. Chem. B*, *2013*, **117**, 8536.
28 I. A. Karpenko, A. S. Klymchenko, S. Gioria, R. Kreder, I. Shulov, P. Villa, Y. Mély, M. Hibert and D. Bonnet, *Chem. Commun.*, *2015*, **51**, 2960.
29 S. Lee, K. K. Y. Yuen, K. A. Jolliffe and J. Yoon, *Chem. Soc. Rev.*, *2015*, **44**, 1749.
30 S. Yang, G. Feng and N. H. Williams, *Org. Biomol. Chem.*, *2012*, **10**, 5606.
31 C. Reichardt, *Angew. Chem. Int. Ed.*, *1979*, **18**, 98.
32 M. Pannipara, A. M. Asiri, K. A. Alamry, M. N. Arshad and S. A. El-Daly, *J. Fluoresc.*, *2014*, **24**, 1629.
33 T. Tiffert and V. L. Lew, *Pflugers Arch.*, *2014*, **466**, 2279.
34 W. Becker, *The world of the cell, 4th ed.* Eds. W. Becker, L. Kleinsmith and J. Hardin, Benjamin Cummings, San Francisco, 2000.
35 F. E. Boas, L. Forman and E. Beutler, *Med. Sci.*, *1998*, **95**, 3077.
36 I. Watanabe and S. Okada, *J. Cell Biol.*, *1967*, **32**, 309.
37 D. Lloyd and C. Williams, *Adv. Microb. Physiol.*, *2015*, **67**, 293.
38 C. G. Mackenzie, J. B. Mackenzie and P. Beck, *J. Biophys. Biochem. Cytol.*, *1961*, **9**, 141.
39 J. Balvan, A. Krizova, J. Gumulec, M. Raudenska, Z. Sladek, M. Sedlackova, P. Babula, M. Sztalmachova, R. Kizek, R. Chmelik and M. Masarik, *PLoS One*, *2015*, **10**, e0121674.
40 K. L. Rock and H. Kono, *Annu. Rev. Pathol.*, *2008*, **3**, 99.
41 A. J. G. Dickinson and L. A. Lowery, *Semin. Cell Dev. Biol.*, *2016*, **51**, 53.
42 J. R. Tata, *Biochem. Cell Biol.*, *1994*, **72**, 581.

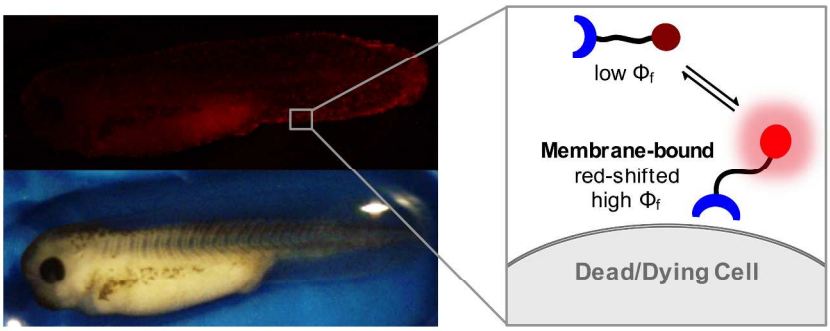

Targeted solvatochromic probe enables non-invasive, time-lapse fluorescence imaging of cell death in cell culture and living frog embryo.